Oseledets' Splitting in Large Hamiltonian Systems: the HMF Phase Transition

M Sala[1, 2] **, A Turchi**[3, 4] **and R Artuso**[1, 2]

1 Center for Nonlinear and Complex Systems & Dipartimento di Scienza ed Alta Tecnologia, Universitá degli Studi dell'Insubria, Via Valleggio 11, 22100 Como, Italia
2 Istituto Nazionale di Fisica Nucleare, Sezione di Milano, Via Celoria 16, 20133 Milano, Italia
3 Dipartimento di Meccanica e Tecnologie Industriali, via Santa Marta 3, 50139 Firenze, Italia
4 Centro Interdipartimentale per lo Studio delle Dinamiche Complesse Via Sansone, 1 - I-50019 , Sesto Fiorentino, Italia

E-mail:
sala.teo1@gmail.com
alessio.turchi@gmail.com
roberto.artuso@uninsubria.it

Abstract.
We consider the covariant Lyapunov vectors (CLV) of a high-dimensional Hamiltonian flow in the case of long range potential, namely the *Hamiltonian Mean Field* (HMF) problem, by studying the behavior of the Lyapunov spectra and the Oseledets' splitting principal angles (the mutual orientation between stable and unstable subspaces) when a phase transition takes place. Motivated by several results connecting the dynamical properties of systems to their Lyapunov exponents and vectors, we first find confirmation of an explicit sensitivity of such quantities to the transition: our main finding is that the mutual orientation between stable and unstable subspaces fluctuates in time around specific constant values. Moreover, the fluctuations statistics are different above and below the critical threshold, and thus intimately connected to the transition. Pictorially, the evolution of the stability subspaces along a reference orbits turns out to happen only through rigid global rotations plus weak internal deformations between the two subspaces; we are not aware of any theoretical explanation for such a non-trivial setting but, through analogies with integrable systems, we provide some little insight on 'how much' the system resembles an integrable one.

1. Introduction

Through this paper we focus on a paradigmatic example of long-range interacting systems, the so called Hamiltonian Mean Field (HMF) model, first introduced by Antoni and Ruffo in 1995 [8] in order to model the behavior of galaxies or plasmas. The HMF is a toy-model that was specifically designed in order to be easily implementable and theoretically studied, thus making it the ideal candidate to investigate the properties of long-range systems in the thermodynamic limit. Since its introduction it has been extensively studied [13], and has become a paradigmatic model for the study of out-of-equilibrium quasi-stationary states (QSS).
The HMF shows an interesting dynamic and thermodynamic behavior: when performing numerical simulations, starting out-of-equilibrium, the system is usually trapped in long-lived QSSs, before relaxing to the Boltzmann equilibrium solution. The QSSs exhibit a breakdown of ergodicity, a distribution of momenta which is non-Maxwellian and anomalous diffusion [9, 10, 11]. The lifetime of these states diverges with the number of degrees of freedom according to a power law, so in the thermodynamic limit they become proper equilibrium states. The simplicity of the model allows one to develop a theoretical approach that explains the presence of QSSs as equilibrium solutions of the Vlasov equation, as pioneered in [12]. However we must note that any finite-size HMF system will eventually thermalize to the Boltzmann equilibrium in a finite time for any choice of initial conditions.
The HMF was also proposed to interpret the behavior of wave-particle interacting systems: under specific conditions its nonequilibrium properties reproduce the dynamical aspects of the Collective Atomic Recoil Laser (CARL) [6].

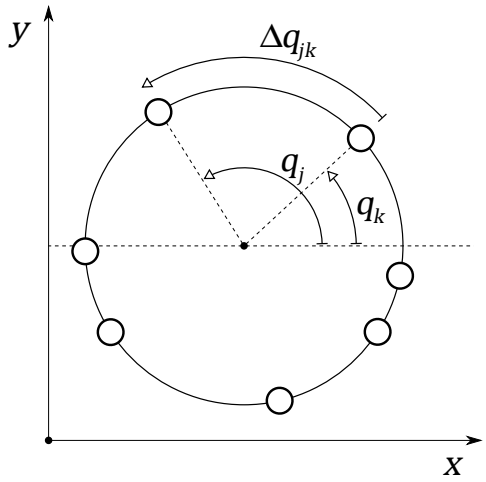

Figure 1. Pictorial presentation of the HMF system, where particles are identified by their angular position q_j over a circle. The interaction is only sensitive to the angular distance Δq_{jk} between each pair of particles.

2. Framework

2.1. The Hamiltonian Mean Field

The HMF model describes N identical particles interacting through cosine potentials:

$$H = \sum_{i=1}^{N} \left[\tfrac{1}{2} p_i^2 + \tfrac{C}{2N} \sum_{j=1}^{N} (1 - \cos(q_i - q_j)) \right] . \tag{1}$$

The canonical coordinate q_i identifies the position of particle i over the unitary circle $[0, 2\pi[$, with periodic boundary conditions, while p_i is the conjugated momentum; since the interaction depends on $\Delta q_{jk} = q_j - q_k$ only (see figure 1) the system is invariant under global rotations around the unit circle and thus the total angular momentum $\bar{p} = \frac{1}{N} \sum_{j=1}^{N} p_j$ is constant (as H) along any trajectory. Notice that, moreover:

- particles have the same mass, which we assume equal to one for simplicity;
- particles can cross each other, or, equivalently, do experience perfectly elastic collisions, in agreement with the hypothesis that masses are identical.

Depending on the value of the coupling constant C, the interaction can be either attractive ($C > 0$) or repulsive ($C < 0$); both cases were studied in the past [13, 14]; in our computations we will consider the case $C = 1$. The HMF potential can be also seen as the first harmonic in the expansion of the one-dimensional self-gravitating potential with periodic boundary conditions [15, 16].
Defining $\dot{} \equiv \frac{\mathrm{d}}{\mathrm{d}t}$ and $\boldsymbol{\nabla}_{\mathbf{q}} \equiv \frac{\partial}{\partial \mathbf{q}}$, the *canonical equations* of motion read:

$$\begin{aligned} &\dot{\mathbf{q}} = \mathbf{p} \ , \\ &\dot{\mathbf{p}} = -\boldsymbol{\nabla}_{\mathbf{q}} V = \ddot{\mathbf{q}} \quad \Rightarrow \quad \ddot{q}_j = \tfrac{C}{N} \sum_{k=1}^{N} \sin(q_k - q_j) \end{aligned} \tag{2}$$

or, denoting $\mathbf{x} = [\mathbf{q}, \mathbf{p}]$ and the velocity field $\mathbf{v}(\mathbf{x}) \equiv [\mathbf{p}, -\boldsymbol{\nabla}_{\mathbf{q}} V]$, dynamics is given by:

$$\dot{\mathbf{x}} = \mathbf{v}(\mathbf{x}) \ . \tag{3}$$

In this case it is then possible to formally write the *Hamiltonian flow* $\mathbf{f}_t$, such that:

$$\dot{\mathbf{f}}_t(\mathbf{x}) \equiv \mathbf{v} \circ \mathbf{f}_t(\mathbf{x}) \quad , \quad \mathbf{f}_t \circ \mathbf{f}_\tau = \mathbf{f}_{t+\tau} \quad , \quad \mathbf{f}_0 = \mathrm{id} \tag{4}$$

for every point $\mathbf{x}$ in the phase space Ω, an orbit is the parametrized curve $\mathbf{x}_t \equiv \mathbf{f}_t(\mathbf{x})$; by definition, velocity field is everywhere tangent to such curve, being the natural direction along which perturbations do not propagate in time.

2.2. Stability

The stability of flow (4) can be investigated by considering infinitesimal perturbations:

$$\delta \mathbf{x}_t = \mathbf{F}_t(\mathbf{x}) \delta \mathbf{x} \ , \tag{5}$$

where the *Jacobian matrices cocyle* is defined as:

$$\mathbf{F}_t(\mathbf{x}) \equiv \left. \tfrac{\partial}{\partial \mathbf{x}} \mathbf{f}_t \right|_{\mathbf{x}} \ ; \tag{6}$$

obviously $\mathbf{F}_0(\mathbf{x}) \equiv \mathbf{1}$ for all $\mathbf{x}$, and the cocycle composition property is sathisfied:

$$\mathbf{F}_t(\mathbf{x}_\tau) \mathbf{F}_\tau(\mathbf{x}) = \mathbf{F}_{t+\tau}(\mathbf{x}) \ . \tag{7}$$

By the latter and from the symplectic structure of Hamilton evolution we get:

$$\mathbf{F}_t(\mathbf{x})^{-1} = \mathbf{F}_{-t}(\mathbf{x}_t) = \mathbf{Y}\,\mathbf{F}_t(\mathbf{x})^T\,\mathbf{Y}^T \quad , \quad \mathbf{Y} \equiv \begin{bmatrix} \mathbf{O} & -\mathbf{I} \\ \mathbf{I} & \mathbf{O} \end{bmatrix} , \tag{8}$$

where $\mathbf{Y}$ is a representation of the fundamental symplectic form. By using (6) and (4) we get:

$$\dot{\mathbf{F}}_t(\mathbf{x}) = \mathbf{K}(\mathbf{x}_t)\mathbf{F}_t(\mathbf{x}) \ , \tag{9}$$

with $\mathbf{K}$ the *stability matrix*, defined as the Jacobian matrix of velocity field $\mathbf{v}$:

$$\mathbf{K}(\mathbf{x}) \equiv \tfrac{\partial}{\partial \mathbf{x}}\mathbf{v}\big|_{\mathbf{x}} \quad , \quad \mathbf{K}(\mathbf{x}_t) \equiv \mathbf{K}_t \ . \tag{10}$$

By deriving (5) w.r.t. time t, we obtain the equations of motion for the perturbations:

$$\dot{\delta\mathbf{x}}_t = \mathbf{K}(\mathbf{x}_t)\delta\mathbf{x}_t \ ; \tag{11}$$

tangent to Ω in $\mathbf{x}_t$ by definition and evolving exactly as each column of matrix $\mathbf{F}_t$. By its structure, both as a matrix and as a function of phase space, $\mathbf{K}$ induces the formal solutions to (9) as *time-ordered exponential* integrals, defined by:

$$\mathbf{F}_t(\mathbf{x}) = \text{T-exp}\left[\int_0^t \mathrm{d}\tau \mathbf{K}(\mathbf{x}_\tau)\right] \equiv \lim_{\tau\to 0}\prod_{k=0}^{t/\tau}\left[\mathbf{1} + \tau\mathbf{K}_{k\tau}\right] \ . \tag{12}$$

with the proper matrix-product ordering; notice that, in general, the exponent *is not* a time-average of the stability matrix unless the latter commutes with itself at different points of the chosen orbit; in such a case we indeed have:

$$[\mathbf{K}_t, \mathbf{K}_\tau] = 0 \quad \Rightarrow \quad \mathbf{F}_t = \mathrm{e}^{t\langle\mathbf{K}\rangle_t(\mathbf{x})} \tag{13}$$

with $[\cdot,\cdot]$ the usual matrix commutator and $\langle\cdot\rangle_t(\mathbf{x})$ the time-average for $\tau \in [0,t]$. Such simplification always occurs in the integrable case of linear velocity fields and, in general, when considering the linearized dinamics of a fixed point; in both cases the stability matrix is constant along the chosen reference orbit (that is, any orbit for the constant system and the fixed point itself) and thus sathisfies (13):

$$\mathbf{K}(\mathbf{x}_t) = \mathbf{K}(\mathbf{x}) = \mathbf{K} \quad \Rightarrow \quad \mathbf{F}_t = \mathrm{e}^{t\mathbf{K}} \equiv \sum_{n=0}^{\infty}\frac{1}{n!}t^n\mathbf{K}^n \ . \tag{14}$$

In this case we can compactly express the spectral problem: we have to find a pair of matrices $\mathbf{\Delta}$, $\mathbf{E}$, with $\mathbf{\Delta}$ diagonal, such that :

$$\mathbf{KE} = \mathbf{E\Delta} \quad , \quad \mathbf{K} = \begin{bmatrix} \mathbf{O} & \mathbf{I} \\ -\mathbf{H} & \mathbf{O} \end{bmatrix} \quad , \quad \mathbf{H} = \tfrac{\partial^2 V}{\partial q^\mu \partial q^\nu} \tag{15}$$

with $\mathbf{O}$, $\mathbf{I}$ and $\mathbf{H} = \mathbf{H}^T$ respectively the null, the identity and the Hessian $N \times N$ matrix of potential V and where we have used (2), (3) and (10). The solution of (15) can then be expressed in terms of $\mathbf{H}$ as follows:

$$\mathbf{E} = \begin{bmatrix} \mathbf{A} & \mathbf{A} \\ \mathbf{A}\boldsymbol{\chi} & -\mathbf{A}\boldsymbol{\chi} \end{bmatrix} \ , \ \mathbf{\Delta} = \begin{bmatrix} \boldsymbol{\chi} & \mathbf{O} \\ \mathbf{O} & -\boldsymbol{\chi} \end{bmatrix} \tag{16}$$

with $\boldsymbol{\chi} = \sqrt{-\mathbf{\Sigma}}$ diagonal and $\mathbf{A}, \mathbf{\Sigma}$ respectively the eigen-vector/values of matrix $\mathbf{H}$:

$$\begin{aligned} &\mathbf{HA} = \mathbf{A\Sigma} \ , \\ &\mathbf{A} = \mathbf{A}^{-T} \ . \end{aligned} \tag{17}$$

Thus the eigenvalues $\chi_k = \sqrt{-\Sigma_k}$ are purely real/imaginary precisely when the real eigenvalues Σ_k , correspondent the principal curvatures of the potential energy surface, are respectively negative/positive; this can be stated by rewriting (14) as:

$$\mathbf{F}_t = \mathrm{e}^{t\mathbf{K}} = \mathbf{E}\,\mathrm{e}^{t\mathbf{\Delta}}\,\mathbf{E}^{-1} \tag{18}$$

showing that $\mathbf{E}$ is an eigenbasis for $\mathbf{F}_t$ at all times, with diagonal action $e^{t\chi_k}$, for each k, corresponding to real exponential contractions/dilations (negative curvatures) or to complex rotations (positive curvatures). This characterizes dynamics (11) completely: the subset $\{\mathbf{e}_k^{\pm}\}$ of real vectors of basis $\mathbf{E}$ corresponding to negative curvatures $\Sigma_k < 0$ are exactly the physical directions along which the system equally contracts and expands, in agreement with its area-preserving nature; indeed, by choosing:

$$\delta\mathbf{x} = \mathbf{e}_k^{\pm} \;\Rightarrow\; \delta\mathbf{x}_t = e^{\pm t\chi_k}\mathbf{e}_k^{\pm} \tag{19}$$

one can see that the set of Lyapunov exponents λ arise [2]:

$$\lim_{t\to\infty} \lambda(\mathbf{x}, \delta\mathbf{x}) \equiv \tfrac{1}{t}\log\frac{\|\delta\mathbf{x}_t\|}{\|\delta\mathbf{x}\|} = \pm\chi_k = \pm\sqrt{-\Sigma_k} \in \mathbb{R}\ . \tag{20}$$

Nonzero Lyapunov exponents are associated with the subset of real eigenvalues of $\mathbf{K}$; this yields the *Lyapunov spectrum* (see figure 2 for an example); the positive curvature directions, associated to imaginary eigenvalues $\pm i|\chi_j|$ instead, extend in the complex domain and yield the principal axes for ellipses in each of the planes (q_j, p_j) invariant under the associated rotations of frequency $|\chi_j|$.

3. Oseledets' Theorem

3.1. Transformed Cocycles

In the generic non-constant nor fixed-point cases, however, the eigenbases of $\mathbf{K}(\mathbf{x})$ evaluated in points along orbits *do not* diagonalize cocycle $\mathbf{F}_t$, as shown by the relation:

$$\mathbf{F}_t(\mathbf{x}) = \mathbf{E}(\mathbf{x}_t)\,\text{T-exp}\left[\int_0^t \mathrm{d}\tau \left(\mathbf{\Delta} - \mathbf{E}^{-1}\dot{\mathbf{E}}\right)(\mathbf{x}_\tau)\right]\,\mathbf{E}(\mathbf{x})^{-1}\ . \tag{21}$$

and (21) reduces to (18) only when $\dot{\mathbf{E}} = \mathbf{O}$, i.e. the eigenbasis is constant along orbits:

$$\dot{\mathbf{E}}(\mathbf{x}) \equiv \tfrac{\mathrm{d}}{\mathrm{d}t}\left[\mathbf{E}\circ\mathbf{f}_t\right]_{t=0}(\mathbf{x}) \ \equiv\ \mathcal{D}_{\mathbf{x}}\mathbf{E} = \mathbf{O}\ ; \tag{22}$$

here $\mathcal{D}_{\mathbf{x}}$ is the *material derivative* for phase-space dependent observables, or, the derivative *along* the flow:

$$\mathcal{D}_{\mathbf{x}} \equiv \sum_{k=1}^{2N} v_j(\mathbf{x})\tfrac{\partial}{\partial x_j} = \sum_{k=1}^{N}\left(p_j\tfrac{\partial}{\partial q_j} - \tfrac{\partial V}{\partial q_j}\tfrac{\partial}{\partial p_j}\right)\ . \tag{23}$$

This fact naturally induces to consider the problem of finding a phase-space dependent basis $\mathbf{U}(\mathbf{x})$ generating a transformed cocycle $\widetilde{\mathbf{F}}_t(\mathbf{x})$:

$$\mathbf{F}_t(\mathbf{x}) = \mathbf{U}(\mathbf{x}_t)\widetilde{\mathbf{F}}_t(\mathbf{x})\mathbf{U}(\mathbf{x})^{-1}\ . \tag{24}$$

and a corresponding transformed stability matrix $\widetilde{\mathbf{K}}(\mathbf{x})$:

$$\widetilde{\mathbf{F}}_t(\mathbf{x}) = \text{T-exp}\left[\int_0^t \mathrm{d}\tau\widetilde{\mathbf{K}}(\mathbf{x}_\tau)\right]\ . \tag{25}$$

constrained to assume some prescribed shape; for example, to obtain a characterization like in (18) for generic systems, one would ask for a diagonal transformed cocycle; combining equations (21) and (24) for a given phase-space dependent basis $\mathbf{U}$ yields:

$$\widetilde{\mathbf{F}}_t(\mathbf{x}) = \text{T-exp}\left[\int_0^t \mathrm{d}\tau\left(\mathbf{U}^{-1}\left(\mathbf{K}\mathbf{U} - \dot{\mathbf{U}}\right)\right)(\mathbf{x}_\tau)\right]\ . \tag{26}$$

and through (25), (26), once given a structure for matrix $\widetilde{\mathbf{K}}$, we obtain:

$$\mathbf{K}\mathbf{U} - \mathcal{D}_{\mathbf{x}}\mathbf{U} = \mathbf{U}\widetilde{\mathbf{K}}\ , \tag{27}$$

that is, a PDE for $\mathbf{U}(\mathbf{x})$ defined over some (possibly dense) subset of phase-space; notice that equation (27) is completely local and time-independent, can have at most $2N$ linearly independent solutions and, when asking for diagonal transformed cocycles and restricted to linear velocities or fixed-points, reduces to the eigen-probem (15).

3.2. Covariant Lyapunov Vectors

The basis $\mathbf{U}$ producing a diagonal transformed cocycle from $\mathbf{F}_t$ is called its *Covariant Lyapunov vectors* basis (CLV), or *Oseledets' splitting*, and is associated to the diagonal transformed stability matrix $\widetilde{\mathbf{K}} = \boldsymbol{\lambda}$ so that equation (27) takes the form:

$$\mathbf{K}\mathbf{U} - \mathcal{D}_{\mathbf{x}}\mathbf{U} = \mathbf{U}\boldsymbol{\lambda}\ . \tag{28}$$

and $\boldsymbol{\lambda}(\mathbf{x})$ is the set of *local exponents* whose time-average determines the new cocycle:

$$\widetilde{\mathbf{F}}_t(\mathbf{x}) = \mathrm{e}^{t\mathbf{\Lambda}_t(\mathbf{x})}\quad,\quad \mathbf{\Lambda}_t(\mathbf{x}) \equiv \langle\boldsymbol{\lambda}\rangle_t(\mathbf{x}) = \tfrac{1}{t}\int_0^t \mathrm{d}\tau\boldsymbol{\lambda}(\mathbf{x}_\tau)\ . \tag{29}$$

In the framework of nonuniformly hyperbolic systems, the *Oseledets' theorem* [3] then states the existence of such precise decomposition of cocycle $\mathbf{F}_t$ into a phase-space dependent 'basis part' $\mathbf{U}$ and a time-dependent 'exponential part' $\mathbf{\Lambda}_t$, such that:

$$\mathbf{F}_t(\mathbf{x}) = \mathbf{U}(\mathbf{x}_t)\, \mathrm{e}^{t\mathbf{\Lambda}_t(\mathbf{x})}\, \mathbf{U}(\mathbf{x})^{-1} \ , \tag{30}$$

where the exponent matrix satisfies the infinite time limit (*Kingman's theorem*, [5]):

$$\lim_{t\to\pm\infty} \mathbf{\Lambda}_t(\mathbf{x}) = \mathbf{\Lambda}\{\mathbf{x}\} \equiv \langle \boldsymbol{\lambda} \rangle_\infty(\mathbf{x}) \ . \tag{31}$$

with $\{\mathbf{x}\} = \{\mathbf{f}_t(\mathbf{x})\}_{t\in\mathbb{R}}$ the *orbit* of $\mathbf{x}$, along which $\mathbf{\Lambda}\{\mathbf{x}\}$ is constant, or, *flow-invariant*. Thus the tangent dynamics exactly maps each vector field $\mathbf{u}_k(\mathbf{x})$ (a column of $\mathbf{U}$) on itself evaluated at a new point, $\mathbf{u}_k(\mathbf{x}_t)$, expanding it by the *same asymptotic* exponent Λ_k in *both* temporal limits [2]; the quantity Λ_k is called the *Lyapunov exponent* associated to the k-th *covariant Lyapunov vector* (CLV), while the sets of all exponents and vectors go respectively under the names of *Lyapunov spectrum* $\mathbf{\Lambda}$ and *Oseledets' splitting* $\mathbf{U}$ of cocycle $\mathbf{F}$, usually ordered by the rule: $_{j<k} \Leftrightarrow \Lambda_j > \Lambda_k$ (as in figure 2). Throughout this paper, positive local exponents will be generically referred to as λ_1, with the label 1 standing for 'one-step' due to the fact that, numerically, such quantities are calculated at every step of the CLV algorithm [24]; in agreement with the second equation in (29), the FTLE Λ calculated over a time t will be labeled $\langle\lambda_1\rangle_t$.

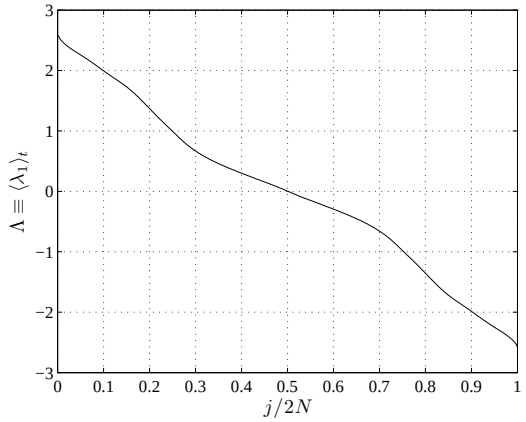

Figure 2. HMF, $N = 256$, $t = 10^7$: Lyapunov spectrum obtained by Benettin's algorithm [7] for the energy density value $\varepsilon = 0.65$; notice that the spectrum is symmetric w.r.t. the normalized index $j = N$, as symplectic property (8) implies.

3.3. Remarks

3.3.1. Ordering In the generic Hamiltonian case, because of the symplectic structure, areas in each (q_k, p_k)-plane are conserved by the flow and the exponents are usually constrained to obey the symmetry: $\Lambda_{2N-k+1} = -\Lambda_{k\ =\ 1\ldots N}$; notice that this condition, as well as the exponents ordering named above, is not fulfilled by the present calculations since, by the convention used here, the matrix of local exponents reads:

$$\boldsymbol{\lambda} = \begin{bmatrix} \hat{\boldsymbol{\lambda}} & \mathbf{O} \\ \mathbf{O} & -\hat{\boldsymbol{\lambda}} \end{bmatrix} \tag{32}$$

with $\hat{\boldsymbol{\lambda}}$ the diagonal matrix containing the positive exponents only; imposing the decreasing ordering on the latter induces an increasing ordering on the negative block, but this is completely unharmful, being equivalent to a global basis permutation and thus factorizable over each considered matrix. In the numerics we apply decreasing ordering to the spectrum, obtaining match with the symplectic condition (figure 2).

3.3.2. Numerical Approximations The search for upper/lower triangular cocycles (implying upper/lower matrices $\widetilde{\mathbf{K}}$) yields orthonormal phase-space dependent bases. The latter are called *Oseledets' orthonormal bases* and can be usually approximated by Benettin's algorithm [7], which by-produces an approximation of the Lyapunov spectrum also; such bases are the same used to perform Ginelli's algorithm [24] to approximate the whole splitting.

3.3.3. Tangencies It should be noticed that the possible existence of solutions $\mathbf{U}$ of equation (27) crucially depends on whether the condition $\det \mathbf{U} \neq 0$ is fulfilled or not, i.e. whether the corresponding column vectors do form a basis; for chaotic Hamiltonian systems this is supposed to hold in the whole phase-space exept for subsets of zero Lebesgue measure, where two or more CLV can coincide, making the matrix $\mathbf{U}$ locally non-invertible. Yet, it is not clear how the effect of such pathological sets, usually called *tangencies*, can affect the dynamics of systems with a large numbers of degrees of freedom; the main problems are connected to the smoothness properties of the flow, that naturally induce the splitting to arbitrarily shrink in points closer and closer to the tangency. In such regions *outside tangencies* the splitting is still invertible but in a numerically weak sense, i.e. all the covariant directions are transversal but some of the *principal angles* between them may be very close to zero (see paragraph 4.2).

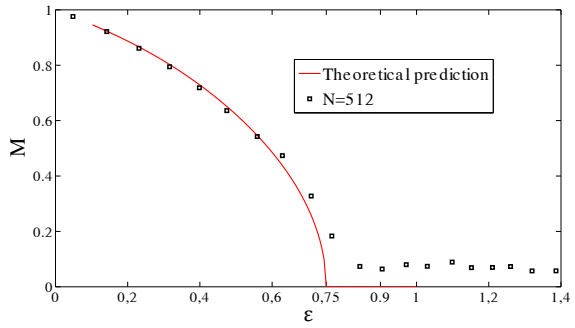

Figure 3. Second order phase transition between homogeneous and magnetized states for the HMF system at equilibrium, at a critical energy per particle $\varepsilon_c = 0.75$. The predicted theoretical curve, displayed by the red thick line, is obtained from the minimization of the free energy in the canonical ensemble. It is consistent with the numerical microcanonical simulations carried out for finite N (the positive magnetization observed in the homogeneous phase is of the order of the finite-size fluctuations $\sim \frac{1}{\sqrt{N}}$).

4. Phase transition

In the following we will focus on the thermodynamical equilibrium description of the HMF model, by studying finite-size systems and avoiding any potential QSS. The simplicity of the HMF allows to obtain analytical solutions for its statistical equilibrium properties, both in the canonical [8] and microcanonical ensemble [13], independently and without relying on ensemble equivalence.
When considering an attractive interaction, the HMF displays a second order ferromagnetic phase transition at equilibrium, which separates homogeneous from inhomogeneous states. In order to characterize this transition we consider the order parameter μ, which is usually referred as the magnetization, in analogy with spin systems, defined as the modulus of the vector $\mathbf{M}$ with axial components M_x M_y as:

$$M_x = \frac{1}{N}\sum_i \cos(q_i) \ , \ M_y = \frac{1}{N}\sum_i \sin(q_i) \ . \tag{33}$$

By defining $\varepsilon = E/N$ as the energy density of the system, the critical value that identify the transition is $\varepsilon_c = 0.75$ (see figure 3), above which magnetization is zero. To study the transition we consider a sampling of 13 values for the energy density:

- below threshold, ε from 0.5 to 0.7 with a step $\Delta\varepsilon = 0.05$ (blue/dashed curves);
- near threshold, $\varepsilon = 0.73$ (green/dashed curves), 0.77 (purple/continuous curves);
- on threshold, $\varepsilon = 0.75$ (black/continuous thick curve);
- above threshold, ε from 0.8 to 1 with a step $\Delta\varepsilon = 0.05$ (red/continuous curves);

the described association between colors/line-types and energy densities is kept constant throughout the paper, as well as the choice of the system parameters: the number of particles, $N = 256$, and the orbits duration, $t = 10^7$, in natural time units.

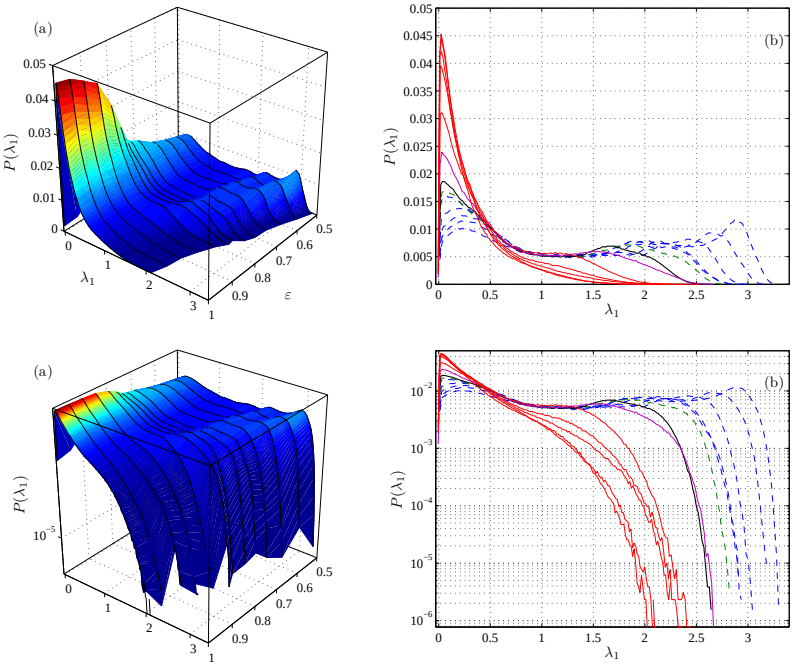

Figure 4. HMF, $N = 256$, $t = 10^7$: total probabilities of all $N - 2$ positive local exponents λ_1 for the 13 energy densities described in chapter 4; two exponents are always 0 due to invariance of the Hamiltonian H and total momentum $\bar{p}$. The distributions have compact support in all cases, but strong modifications occur along the transition: below treshold the range of local exponents is broader (being higher the largest LE, see figures in 5 and 11 for $j = 1$), giving rise to a plateau with several maxima, disappearing as the critical energy is approached; above the transition probability accumulates on the only maximum remaining, located in $\lambda_1 = 0$. This is already a rough argument supporting the fact that the disordered phase is far less unstable than the orderd one [17], although arbitrarily small FTLE never disappear from the latter (see again figures 5, 11 for $j = N$). Notice that negative λ_1 values in these pictures are due to fluctuating violations of the symplectic condition (8); such fluctuations, although very small and decreasing as $1/t$, are stronger and last longer when the stability is weaker, i.e. above threshold.

4.1. Lyapunov spectrum

As a first test to probe the sensitivity of tangent dynamics on the phase transition, we consider the distribution $P(\lambda_1)$ for the set of first $N - 2$ local exponents λ_1, i.e. the nonzero ones, discarding for now the information associated to the spectrum label j. By inspecting figure 4 we notice that some qualitative features change between the two phases: while in the homogeneous phase the distribution looks like an antisymmetric bell around $\lambda_1 = 0$, an instability plateau appears below the critical threshold; in all cases the distribution have compact support, by definition, over λ_1 positive values.
It was as already noticed [17], from numerical analysis, that the first local exponent exhibits anomalous fluctuations when below threshold, increases with energy up to ε_c, while for $\varepsilon > \varepsilon_c$ it goes to zero. The time averages of λ_1 for each value of the FTLE spectrum index j are then organized in figure 5, showing that the ordered phase has larger exponents than the disordered one, although arbitrarily small values persist

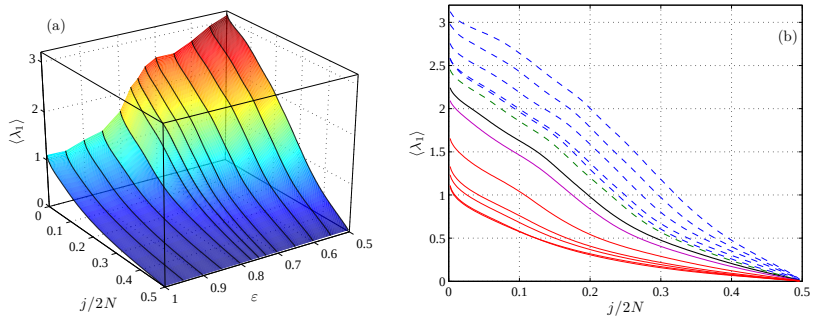

Figure 5. HMF, $N = 256$, $t = 10^7$, positive Lyapunov spectra for the considered 13 as described in chapter 4; a steep decay in the instability is apparent exactly above the transition $\varepsilon = 0.75$, with a decrease of the whole spectrum and important attenuations on the larger exponents. Arbitrary small exponents persist at all phases and are tipically responsible for anomalous statistical features of the dynamics, as shown by λ_1 variances in the next figure.

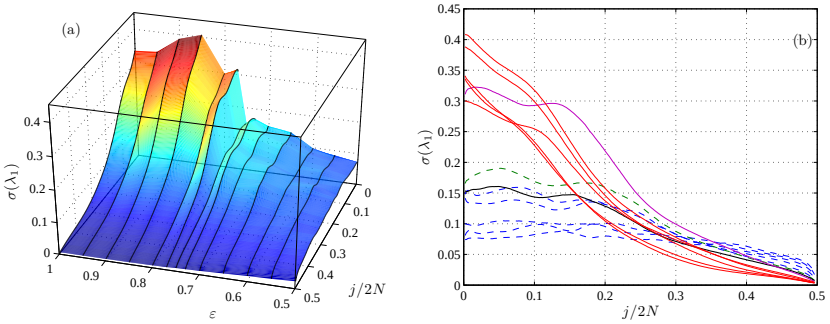

Figure 6. HMF, $N = 256$, $t = 10^7$: time variances of the positive local exponent λ_1 for 13 values of the energy density ε as described in chapter 4; such quantities measure the broadness of fluctuations (decaying as $1/t$) of each FTLE (see also figure 11). The transition changes the exponents statistics from a more uniform situation, where the fluctuations over all exponents are comparable (magnetized phase, blue/dashed curves), to a situation in which the small and intermediate exponents fluctuates much less than the large ones (disordered phase, red/continuous curves).

at all phases. Fluctuations in time of the FTLE spectra are also sensitive to the transition, as shown by the variances $\sigma(\lambda_1)$ in figure 6; in the disordered phase, large exponents have much stronger fluctuations than the intermediate and small ones, while in the magnetized phase the exponents tend to fluctuate more uniformly. Finite size effects are also important: in the limit of infinite size $N \to \infty$ the *largest Lyapunov exponent* (LLE) drops to zero with a power law scaling $N^{-\frac{1}{3}}$ [18]. An analytical estimate of the scaling of the LLE was proposed [23], which uses a geometrical method based on microcanonical averages [19], and the same law was also obtained from a random matrix approach [21]; the model was shown to move towards integrability for N large also in [22]. A study of the scaling properties of the Lyapunov spectrum and of the Kolmogorov-Sinai entropy was performed in [20].

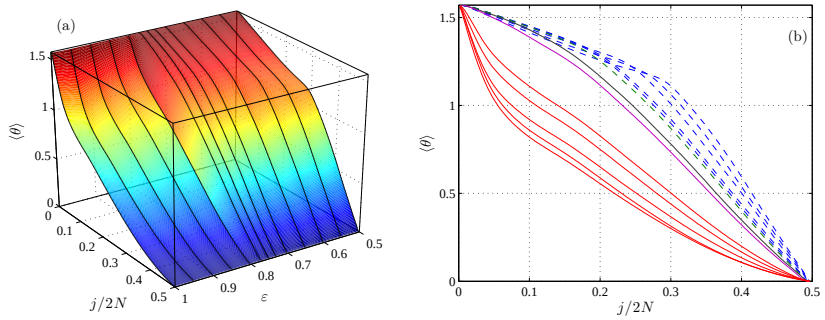

Figure 7. HMF, $N = 256$, $t = 10^7$: Principal angles for 13 values of the energy density ε as described in chapter 4, showing a qualitative change across the transition, with persistency of arbitrarily small angles above and below $\varepsilon_c = 0.75$.

4.2. Principal Angles & Hamiltonian Stability

We now proceed to illustrate our main numerical findings, by probing geometric features of tangent dynamics. As already mentioned, when some of the covariant vectors take very similar directions it is possible that, nearby, there exist points in which the splitting is not invertible, i.e. *tangencies* appear. In general, given two sets both spanned by $n < 2N$ *unit vectors* in $\mathbb{R}^{2N}$, the *reciprocal orientation* between the two is defined by the so called *principal angles* (PA), defined recursively, from the smallest to the largest, as the smaller possible angles between the two subspaces [4]. More explicitly, writing the two sets of vectors as $2N \times n$ matrices $\mathbf{U}$ and $\mathbf{S}$, such angles then correspond to the singular values of the matrix product:

$$\mathbf{U}^T\mathbf{S} = \mathbf{A}\mathbf{Z}\mathbf{B}^T \quad , \quad \mathbf{Z} = \mathrm{diag}(\cos(\theta_j))_{j=1\ldots n} \tag{34}$$

with the *singular values decomposition* (SVD) of product $\mathbf{U}^T\mathbf{S}$ on the r.h.s. of the first equation; the two basis matrices $\mathbf{A}$, $\mathbf{B}$ are orthogonal and, along with the diagonal matrix $\mathbf{Z}$ of real eigenvalues, they diagonalize the two symmetric matrices:

$$\mathbf{U}^T\mathbf{S}\mathbf{S}^T\mathbf{U} = \mathbf{A}\mathbf{Z}^2\mathbf{A}^T \quad , \quad \mathbf{S}^T\mathbf{U}\mathbf{U}^T\mathbf{S} = \mathbf{B}\mathbf{Z}^2\mathbf{B}^T \tag{35}$$

In the present work, in order to probe the *hyperbolicity* of the system, we compute the PA between the stable and unstable CLV, i.e. the pair of $2N \times N$ matrices composing by blocks the CLV matrix, $\mathbf{U} = [\mathbf{U}_+, \mathbf{U}_-]$. In figure 7 the spectra of principal angles are shown for the 13 values of the energy density already described in this chapter; we notice a strong qualitative change in the angles profiles, with a flip of the sign of the concavity as the main feature. On the other hand, both above and below the transition there are arbitrarily small angles, meaning that the system remains nonuniformly hyperbolic for all energy densities; in other words, tangencies or almost-tangencies are always present between the stable and unstable subspaces, in agreement with the fact that for all energy values there are arbitrarily small FTLE (see figure 5). Notice also the extremely low amplitude of fluctuations (see figure 12 for an overlook); this feature is strong in the ordered phase. This is a very subtle property: apparently, tangent subspaces respectively spanned by the stable/unstable CLV correspond to structures whose reciprocal orientation is very rigid. Practically speaking, this means that the splitting changes along a reference orbit through arbitrary global rotations (i.e. all the vectors rotate through the same matrix, leaving the splitting undeformed) plus very weak *internal* deformations.

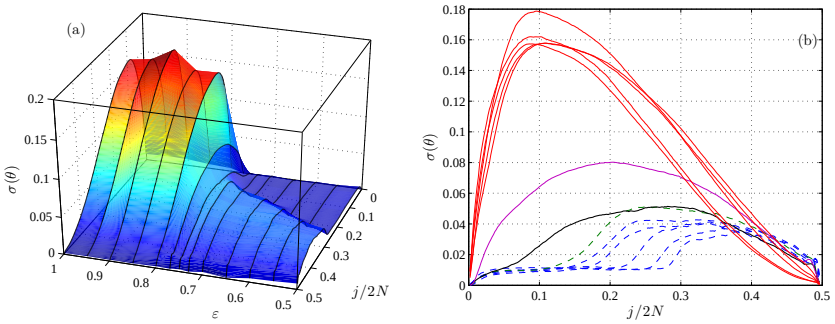

Figure 8. HMF, $N = 256$, $t = 10^7$: time variances of the principal angles for 13 energy densities as described in chapter 4 and for all the angles $\{\theta_j\}_{j=1...N}$; notice the huge qualitative and quantitave variation across the transition: below the threshold, in the disordered phase, all the fluctuations are very low, while exactly across the transition ($\varepsilon = 0.75$, black/continuous thick curve), and above, the spectrum fluctuates by one order of magnitude more; interestingly, in the disordered phase ($\varepsilon < 0.75$) there can be identified a subset of the spectrum, $j \in [1, j^*]$, that shrinks to zero while moving toward the transition and in which the angles (from the largest to θ_{j^*}) have very low fluctuations; although surely connected to the geometrical aspects of the transition, this last fact remains subtle to explain due to its statistical nature.

4.3. Principal Angles for Fixed Points

The small fluctuations of principal angles suggest to explicitly calculate them for fixed points, with $\mathbf{K}$ constant and $\mathbf{U} = \mathbf{E}$ as in (16) and (17); by taking into account that each column of $\mathbf{E}$ is normalized to 1 by the factor $1 + \Sigma_j$, decomposition (34) reads:

$$\hat{\mathbf{E}}^T \hat{\mathbf{E}} = \begin{bmatrix} \mathbf{U}_+^T \mathbf{U}_+ & \mathbf{U}_+^T \mathbf{U}_- \\ \mathbf{U}_-^T \mathbf{U}_+ & \mathbf{U}_-^T \mathbf{U}_- \end{bmatrix} = \begin{bmatrix} \mathbf{I} & \mathbf{W} \\ \mathbf{W} & \mathbf{I} \end{bmatrix} ; \tag{36}$$

$$\mathbf{W}_{jj} = \frac{1 + \Sigma_j}{1 - \Sigma_j} = \frac{1 - \chi_j^2}{1 + \chi_j^2} , \tag{37}$$

with $\mathbf{W}$ diagonal, χ_j a real eigenvalue of $\mathbf{K}$ and Σ_j the corresponding negative principal curvature/eigenvalue of the Hessian matrix $\mathbf{H}$ of potential V; since the singular decomposition of each (in this particular case, diagonal) block matrix yields the identity matrix as orthonormal bases, matrix $\mathbf{W}$ contains itself the singular values and thus the cosines of pricipal angles between stable $\mathbf{U}_-$ and unstable $\mathbf{U}_+$ subspaces:

$$\cos(\theta_j) = \frac{1 - \chi_j^2}{1 + \chi_j^2} \tag{38}$$

yielding a relation between principal angles and local exponents, that in this case correspond to the exact Lyapunov spectrum Λ_j.
Such relation between principal angles and Lyapunov spectrum is a very interesting property that, in principle, can be tested over any Hamiltonian system once the spectra of exponents and angles are known; since the relation holds exactly for potentials that are quadratic functions of the configurational coordinates q, here we quantify how much the system deviates from a quadratic one by the difference:

$$R_j = \cos(\,\langle \theta_j \rangle\,) - \frac{1 - \langle \lambda_1^j \rangle^2}{1 + \langle \lambda_1^j \rangle^2} ; \tag{39}$$

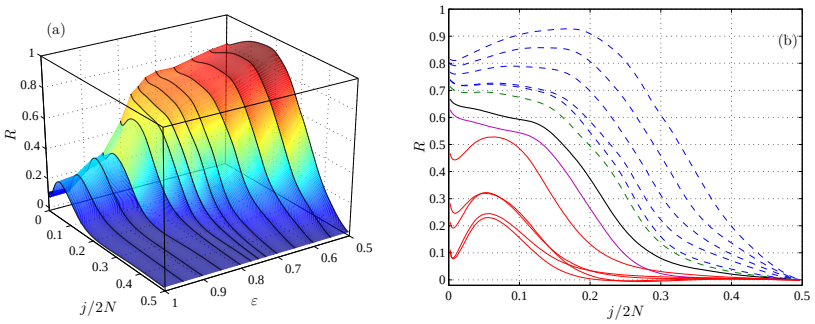

Figure 9. HMF, $N = 256$, $t = 10^7$: the difference R in equation (39) for the 13 values of the energy density as described in chapter 4; the FTLE spectrum, obtained by time averages $\langle\lambda_1\rangle_t$, is treated as the set of eigenvalues of some Hessian matrix $\mathbf{H}$ that is constant in phase space, i.e. corresponds to some potential V that is *quadratic* in the q coordinates. When the system is truly quadratic, $R = 0$ for all the spectrum; here we find that, above threshold ($\varepsilon > \varepsilon_c$, purple and red continuous curves) large subsets of the FTLE and principal angles spectra behave as in a quadratic system.

obtained by the time-averages of both the angles spectrum and the local exponents spectrum; figure 9 shows that the system never coincides with a purely quadratic one but, once above threshold $\varepsilon_c = 0.75$, becomes nearer and nearer to it, with larger and larger portions of the spectra having R falling near zero. This can be seen by plotting the RMS of R (over j) versus the order parameter, figure 10, fitting well a linear profile with slope ~ 1 that, interestingly, localizes the RMS vanishing point at $\mu = 0$. These facts suggest that, in the ordered phase, the tangent structure of the system is not uniform across phase space although the reciprocal orientation between stable/unstable subspaces is rigid; on the contrary the disordered phase, characterized by larger internal fluctuations, has a large subset of tangent subspaces that behave as in a uniform, quadratic system.

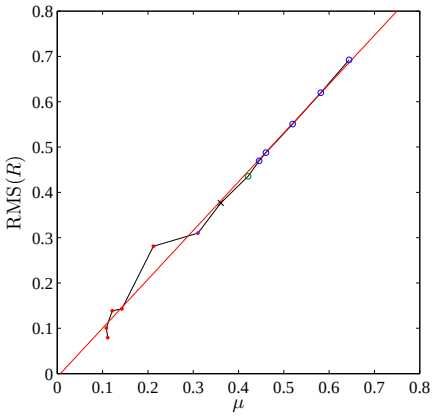

Figure 10. HMF, $N = 256$, $t = 10^7$: scatter plot of the the root mean square of R over j (39) VS the order parameter μ, for the 13 values of the energy density as described in chapter 4 with the correspondence: below threshold (dots), on threshold (cross) and above threshold (circles); we find good agreement with a linear fit (red line) with slope ~ 1, that gives a vanishing RMS point at $\mu = 0$. Notice that in all the performed simulations the resulting RMS is nonzero, in agreement with the fact that the system under study never generates a true quadratic effective potential but, as shown here, deviates from it by a quantity highly correlated with the order parameter of the system.

5. Conclusions

We considered the Hamiltonian Mean Field problem for a range of energy density ε from below to above the analytic critical value $\varepsilon_c = 0.75$, calculating for each case both the Lyapunov exponents and the Oseledets' splitting principal angles spectra; the sensitivity of the whole Lyapunov spectrum to the phase transition is confirmed, with strong correlations with the behavior of magnetization μ (the order parameter of the system). Our main result is that a dynamical analysis in terms of the Oseledets' splitting angles turns out to provide a clearer dynamical signature of the phase transition, with respect to more conventional indicators based on the Lyapunov spectrum only. Through extensive numerical investigations, we find that stable/unstable subspaces in the $\mu \neq 0$ phase obey to a nontrivial constraint for which the two tangent subsets (evaluated pointwise along some reference orbit) mantain a rigid reciprocal orientation that can only fluctuate very weakly in time.

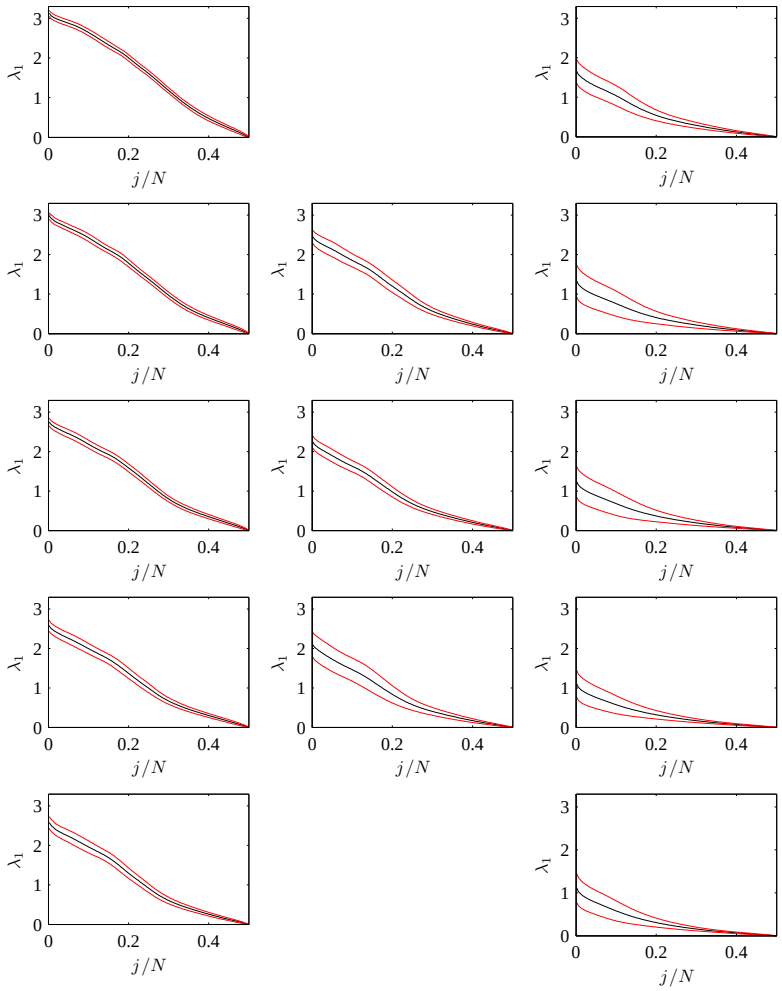

Figure 11. HMF, $N = 256$, $t = 10^7$: time-average (black curves) and time-average$\pm$variance (red curves) of local exponent λ_1 spectra for the considered energy density values: $\varepsilon = 0.50, 0.55, 0.60, 0.65, 0.70$ (resp. from upper panel in left column), $\varepsilon = 0.73, 0.75, 0.77$ (resp. from upper panel in central column) and $\varepsilon = 0.80, 0.85, 0.90, 0.95, 1.00$, (resp. from upper panel in right column), i.e. the same graphs of figure 5, with superimposed the fluctuations obtained by the variances in (6); the phase transition ($\varepsilon_c = 0.75$, central panel) induces modifications both in the maximal value of the spectra (in $j = 1$ or $j/2N \to 0$, by definition) and in the behavior of the corresponding variances. Above the transition (all right column and lower panel in central column) fluctuations are overall wider than below, while the maximal instability is weaker.

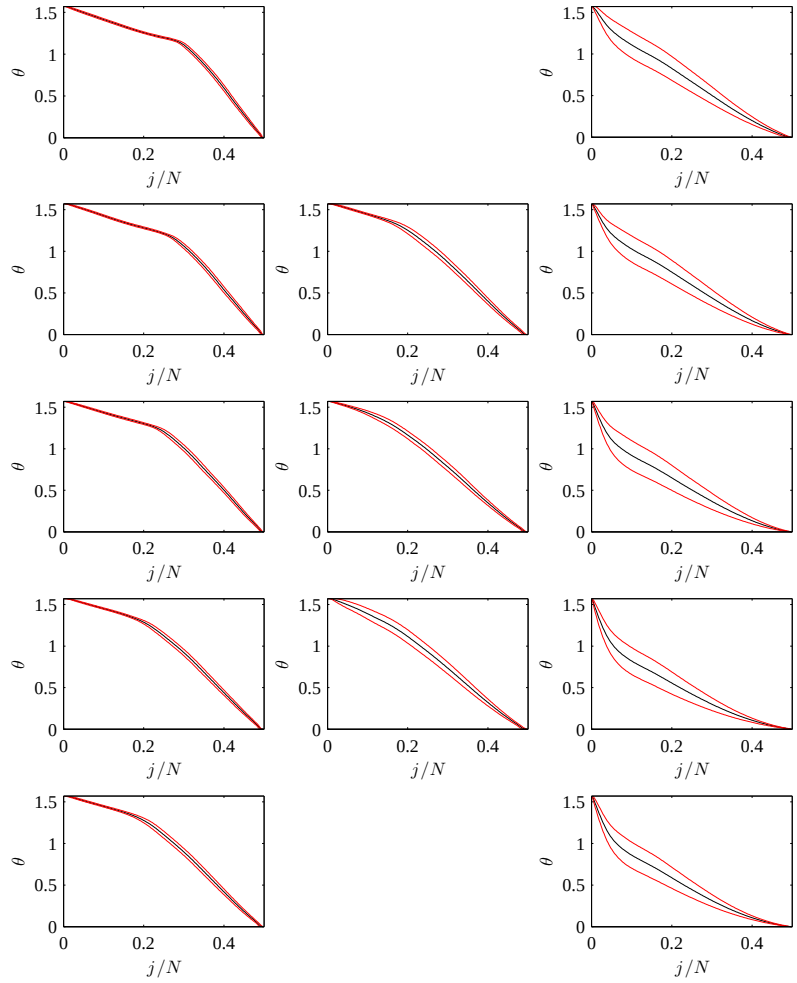

Figure 12. HMF: time-average (black curves) and time-variance (red curves) of principal angle spectra for the considered energy density values: $\varepsilon = 0.50$, 0.55, 0.60, 0.65, 0.70 (resp. from upper panel in left column), $\varepsilon = 0.73$, 0.75, 0.77 (resp. from upper panel in central column) and $\varepsilon = 0.80$, 0.85, 0.90, 0.95, 1.00, (resp. from upper panel in right column); the transition is apparent through the variances of the spectra: indeed, for energies below threshold ($\varepsilon < \varepsilon_c = 0.75$, all left column and upper panel in central column) the fluctuations around the average are very small. Above threshold, instead, fluctuations rise significantly, while the concavity of the average spectra flips its sign; notice that in all dynamical regimes the largest/smallest angles share small fluctuations, indicating that the upper/lower bounds for the splitting amplitude are practically constant and the fluctuations in the geometry of stable/unstable subspaces affects mainly the intermediate angles.

References

[1] A.M. Lyapunov, *The general problem of the stability of motion*, Taylor & Francis, 1992.
[2] L. Barreira, Y. B. Pesin, *Lyapunov exponents and smooth ergodic theory*, University Lecture Series, Am. Math. Soc. (2002).
[3] V.I. Oseledets, Trans. Moscow Math. Soc. **19**, 197-231 (1968).
[4] Kuptsov, P. V. & Kuznetsov, S. P. , Phys. Rev. E **80**, 016205 (2009).
[5] J. F. C. Kingman, J. Roy. Statist. Soc. Ser. B, **30**: 499-510 (1968).
[6] R. Bachelard, T. Manos, P. de Buy, F. Staniscia, F. S. Cataliotti, G. De Ninno, D. Fanelli, N. Piovella, J. Stat. Mech. P06009 (2010).
[7] G. Benettin, L. Galgani, A. Giorgilli, and J. M. Strelcyn, Meccanica **15**, 930 (1980).
[8] M. Antoni, S. Ruffo, Physical Review E **52**, 2361 (1995).
[9] V. Latora, A. Rapisarda, S. Ruffo, Physica A **280**, 81 (2000)
[10] V. Latora, A. Rapisarda, S. Ruffo, Phys. Rev. Lett. **83**, 2104 (1999).
[11] A. Giansanti, D. Moroni, A. Campa, Chaos, Solitons and Fractals **13**, 407 (2002).
[12] A. Antoniazzi, F. Califano, D. Fanelli, S. Ruffo, Phys. Rev. Lett. **98**, 150602 (2007).
[13] A. Campa, T. Dauxois, S. Ruffo, Physics Reports **480**, 57 (2009).
[14] J. Barr, F. Bouchet, T. Dauxois, S. Ruffo, Phys. Rev. Lett. **89**, 110601 (2002).
[15] T. Konishi, K. Kaneko, J. Phys. A **25**, 6283 (1992).
[16] J. Barré, *Mécanique Statistique et Dynamique Hors Equilibre de Systémes avec Interaction à Longue Portée*, PhD Thesis (2003).
[17] Y. Y. Yamaguchi, Prog. Theor. Phys. Suppl. **95**, 717 (1996).
[18] V. Latora, A. Rapisarda, S. Ruffo, Phys. Rev. Lett. **80**, 692 (1998).
[19] M. Pettini, *Geometry and Topology in Hamiltonian Dynamics and Statistical Mechanics, Interdisciplinary Applied Mathematics* vol. **33**, Springer, New York (2007).
[20] V. Latora, A. Rapisarda, S. Ruffo, Physica D **131**, 38 (1999).
[21] M.C. Firpo, S. Ruffo, J. Phys. A: Math. Gen. **34** L511 (2001).
[22] R. Bachelard, C. Chandre, D. Fanelli, X. Leoncini, S. Ruffo, Phys. Rev. Lett. **101** 260603 (2008).
[23] M. C. Firpo, Phys. Rev. E **57**, 6599 (1998).
[24] F. Ginelli, A. Turchi, Politi, Phys. Rev. Lett. **65** 016210 (2001).